

Physico-electrical properties of starch-based bioplastic enhanced with acid-treated cellulose and graphene oxide fillers

Olugbenga Oluwasina^{a,*}, Abiodun Aderibigbe^{a,b}, Stephen Ikupoluyi^a, Olayinka Oluwasina^{c,d}, Theophilus Ewetumo^e

^a Department of Chemistry, Federal University of Technology Akure, Akure, Ondo State P.M.B. 704, Nigeria

^b Department of Chemistry, University of Warwick, Coventry CV4 7AL, United Kingdom

^c School of Chemistry and Physics, University of KwaZulu-Natal, Westville Campus, Private Bag X54001, 4000, South Africa

^d Department of Marine Science and Technology, Federal University of Technology Akure, Akure, Ondo State P.M.B. 704, Nigeria

^e Department of Physics, Federal University of Technology Akure, Akure, Ondo State P.M.B. 704, Nigeria



ARTICLE INFO

Keywords:

Conductive bioplastic
Cellulose
Graphite-rod
Graphene oxide
Luffa cylindrica
Starch

ABSTRACT

Biopolymer composites represent an emerging alternative to petroleum-derived polymers for applications in electronic devices. Cellulose from Luffa cylindrical was treated with acid, and graphene oxide was produced from waste battery rod graphite. The two products were characterized using FTIR, SEM, TGA and XRD. After that, starch-based bioplastic films with varying amounts of acid-treated cellulose (ALC-cellulose) and graphene oxide (GO) as fillers were prepared, and the physical and electrical properties were determined. XRD data revealed a crystallinity of 62% for the ALC-cellulose and 52% for the cellulose precursor. GO had a *d*-spacing of 0.76 nm compared to 0.29 nm for battery-sourced graphite. TEM micrograph analyses revealed an average fibre diameter of 44.7 nm for acid-treated cellulose and 99.7 nm for cellulose. The density, thickness, opacity, and tensile strength of the bioplastic films increased from 1.31 to 1.44 g/cm³, 0.21–0.48 mm, 14.78–38.64, and 0.98–1.42 MPa, respectively, while the moisture content, swelling ability, and porosity reduced, with an increase in percentage composition of the filler materials. The dielectric constant and conductivity increased from 50.3 to 6965.2 and 0.0036–0.0147 S/m with an increase in percentage composition of the filler materials except for Film_{cr4}, which showed a drop in dielectric constant (3033.73) and conductivity (0.0074 S/m). Overall, this study has demonstrated that bioplastic filler materials can be sourced from waste materials and that these fillers improved the starch-based bioplastic film's physical and electrical properties.

1. Introduction

Environmental pollution and climate change effects have been linked to the production and use of petroleum-derived plastics [1]. Nearly every stage in the production process of petroleum-derived plastics involves the release of greenhouse gases and toxic chemicals. Worse still, petroleum-derived plastics are stable to degradation, and some remain intact for as long as 60 years, a situation implicated in ocean plastic pollution. Much research has been directed to preparing and testing biomass-derived bioplastics with comparable properties to petroleum-derived ones to reduce the ecological problems of producing and using petroleum-derived plastics [2,3]. Bioplastics are materials made entirely or partly from renewable biomass or microbes, primarily biodegradable, sustainable, and biocompatible [4]. Bioplastics have

been sourced from many renewable biomasses, including starch, cellulose, chitosan, casein, wheat, agar, and carrageen [5,6]. However, neat bioplastics' relatively poor mechanical and electrical properties have necessitated exploring filler materials to improve these properties [7,8]. Starch-based bioplastic samples from various sources have also been fortified with metal-containing filler materials to improve electrical conductivity [9]. For instance, starch-based bioplastic samples with lithium perchlorate filler showed higher electrical conductivity than those without lithium perchlorate [10]. Carbon-based materials have proved effective in improving bioplastic properties. Recently, graphene synthesized by the electrochemical-mechanical liquid exfoliation of graphite was used as a filler material for tapioca-derived starch bioplastic to access a starch/graphene conductive bioplastic composite. It was observed that the mechanical properties of the composite, mainly

* Corresponding author.

E-mail address: oooluwasina@futa.edu.ng (O. Oluwasina).

Young's modulus and tensile strength, increased with an increase in the added filler graphene. Interestingly, the conductivity of the bioplastic composite was better than that of the parent starch material [1].

Though graphene has exceptional electrical conductivity, high surface area, and excellent mechanical properties and has been applied in electrochemical double-layer capacitors (E.D.L.C.s), sensors, field-effect transistors, power and energy fields, and composite polymer [11,12], it is relatively expensive and difficult to synthesize leading to the search for cheaper and structurally identical alternatives like graphene oxide (GO) [1]. GO comprises a graphene layer bearing oxygen-containing functional groups and has been prepared by treating graphite with potent oxidizing agents [13]. The hydrophilic nature of GO allows its dispersibility in other matrices like starch [14]. The electrical conductivity of GO-derived polymers such as graphene oxide/polypyrrole [15] and graphene oxide/polyaniline [16] has been exploited. Although graphite can be exploited from natural deposits or prepared synthetically, the high cost involved has led to sourcing the material from end-of-life materials like waste from zinc-carbon batteries [17]. Worldwide, 12 and 40 billion primary non-rechargeable batteries were sold in 1993 and 2006, respectively [18]. The commonest of these batteries is the Leclanche zinc-carbon type composed of graphite rod, manganese dioxide, zinc chloride, and ammonium chloride [19]. The epileptic power supply in most parts of Nigeria has made zinc-carbon Leclanche batteries a popular commodity because of their low price and cheap electric provision. However, the high demand in usage and the single-use characteristic of this battery, caused it to be one of the solid waste materials in the country. The spent Leclanche zinc-carbon batteries constitute an environmental nuisance and a potential household hazard due to lead, cadmium, mercury, and manganese poisoning. The high graphite content in the components of the spent zinc-carbon Leclanche necessitates recycling and re-use [19].

Luffa cylindrica (L.) is cultivated in South America and Asia for medicinal and edible purposes [20]. *Luffa cylindrica* L. has impressive strength, toughness, and a mat-forming nature [21]. Isolation of cellulose from *Luffa cylindrica* has been reported by Adewuyi and Pereira [22], while 65% extraction has been achieved by Seki et al. [23]. In Nigeria, *Luffa cylindrica* is an uncultivated wild plant that is underutilized and mainly used as a sponge for bathing or plate washing. Fibre surface modification is essential for composite preparation, and chemical fibre modification has produced various cellulose derivatives such as microcrystalline cellulose, nanocrystalline cellulose, and microfibrillated cellulose. These have better mechanical properties and lower moisture uptake than untreated cellulose. For example, alkaline-treated *Luffa cylindrica* improved the mechanical properties of epoxy composites [24]. At the same time, Agustin and coauthors [25] reported that starch-based bioplastic reinforced with cellulose nanocrystal filler material demonstrated better mechanical properties than raw starch films. Microcrystalline cellulose has been used as a reinforcement agent in starch, soya, agar, polyvinyl alcohol, and polylactic acid [26] bioplastic film composites. Microfibrillated cellulose has also been incorporated into starch, polypropylene carbonate, and polyvinyl alcohol [27,28], with the composites showing improved properties compared to the raw materials.

The eco-environmental nuisance, the threat to humans, plants and living organisms of synthetic conducting polymers, has prompted the search for a suitable substitute. Research on developing conducting polymers has shifted to using biopolymers and biocompatible conductive materials to produce biodegradable bio-conducting polymers [29]. The enormous importance of conducting polymers cannot be overemphasized because these polymers have been found helpful in fields like medical, environmental, agricultural, pharmaceutical, electrical, engineering and food processing [30]. Polymers like protein, polysaccharide, and bio-gum have been utilized while conducting materials like polyaniline, polypyrrole, and polythiophene have been used for conducting polymer Preparation [31].

While several types of filler materials have been incorporated into

starch to prepare conductive bioplastic films, more studies need to investigate filler materials sourced from renewable materials and waste products. Therefore, for the first time, we report on the preparation and investigation of the physical and electrical properties of starch-based bioplastic films fortified with fillers prepared from waste products (waste dry cell battery) and renewable biomass (*Luffa cylindrica* L.). The physical properties determined include density, moisture content, opacity, swelling ability, water absorption rate, porosity, and crystallinity index. Mechanical properties investigated are tensile strength, elongation at break, and Young's modulus. Dielectric constant and conductivity are the electrical properties investigated. This work is a proof of concept for developing conductive bioplastic films for next-generation applications in portable electrical devices.

2. Experimental section

2.1. Materials and chemicals

The *Luffa cylindrica* (L.C.) fruit was sourced from an open greenfield site near a commercial sawmill in Ore, Ondo State, Nigeria. Starch prepared from cassava (*Manihot esculenta* Crantz) was sourced from the leftovers in a different study by Oluwasina et al. [32]. Waste dry cell batteries were collected from household bins in Araromi-Obu, Nigeria. Sodium hydroxide (NaOH), sodium chlorite (NaClO₂), hydrogen peroxide (H₂O₂, 32%), glycerin, sulfuric acid (H₂SO₄, 98%), glacial ethanoic acid (CH₃COOH), phosphoric acid (H₃PO₄), and sodium borohydride (NaBH₄) were purchased from Sigma-Aldrich. Potassium permanganate (KMnO₄), hydrochloric acid (HCl, 35%), and trisodium citrate were bought from BDH Analytical Chemicals (United States).

2.2. Preparation of ALC-cellulose

The acid-treated *Luffa cylindrica* cellulose (ALC-cellulose) was prepared from the *Luffa cylindrica* fruit (LC-fruit) following the method of Oluwasina et al. [33]. Briefly, the LC-fruit pod was cleaned, dehulled, deseeded, and the spongy fruit obtained was cut into pieces, pulverized, and screened through a mesh, and particle size ranging from 250 to 450 µm was collected and stored in a dry container. This was followed by pulping. Typically, pulping was undertaken by boiling 20 g of LC-fruit in 0.4 L sodium hydroxide at 120 °C for 1.5 h. The resulting suspension was left to cool, and the pulp was separated by filtration. The pulp was washed with water until a neutral pH was achieved. Finally, the pulp was dried in an oven at 105 °C until a constant weight was achieved. The pulp was bleached by heating a mixture of pulp, hot distilled water, sodium chlorite, and acetic acid in the ratio 1:50:0.5:0.13 by mass respectively at 70 °C for 1 h followed by the addition of a fresh batch of sodium chlorite (10 g) and acetic acid (0.0025 L) and heating for another 1 h. The reaction was quenched by the addition of distilled water (0.5 L) and allowed to cool before the resulting product was filtered, washed with distilled water until a filtrate with neutral pH was obtained, and finally dried at 105 °C to yield the bleached sample labelled as LC-cellulose. The LC-cellulose (20 g) was treated with H₂SO₄ (0.4 L, 30%) at 55 °C for 30 min under constant stirring (Fig. 1). The residue was washed with H₂O (2 L) to neutral pH, filtered and dried at 70 °C, and labelled as acid-treated cellulose (ALC-cellulose).

2.3. Preparation of graphene oxide

The graphene oxide (GO) was prepared from graphite rods separated from waste dry cell batteries. The graphite rods were washed with H₂O, dried, milled (using a ball mill) into flakes, and sieved. A mixture of the graphite flakes (1.5 g, 125–180 µm), concentrated sulfuric acid (60 mL, 98%), and phosphoric acid (10 mL, 85%) in a round-bottomed flask partially immersed in an ice bath was added KMnO₄ (12.0 g) slowly for 1 h [34]. The reaction mixture was left to warm to room temperature and then warmed at 55 °C for 6 h. This was followed by adding H₂O₂

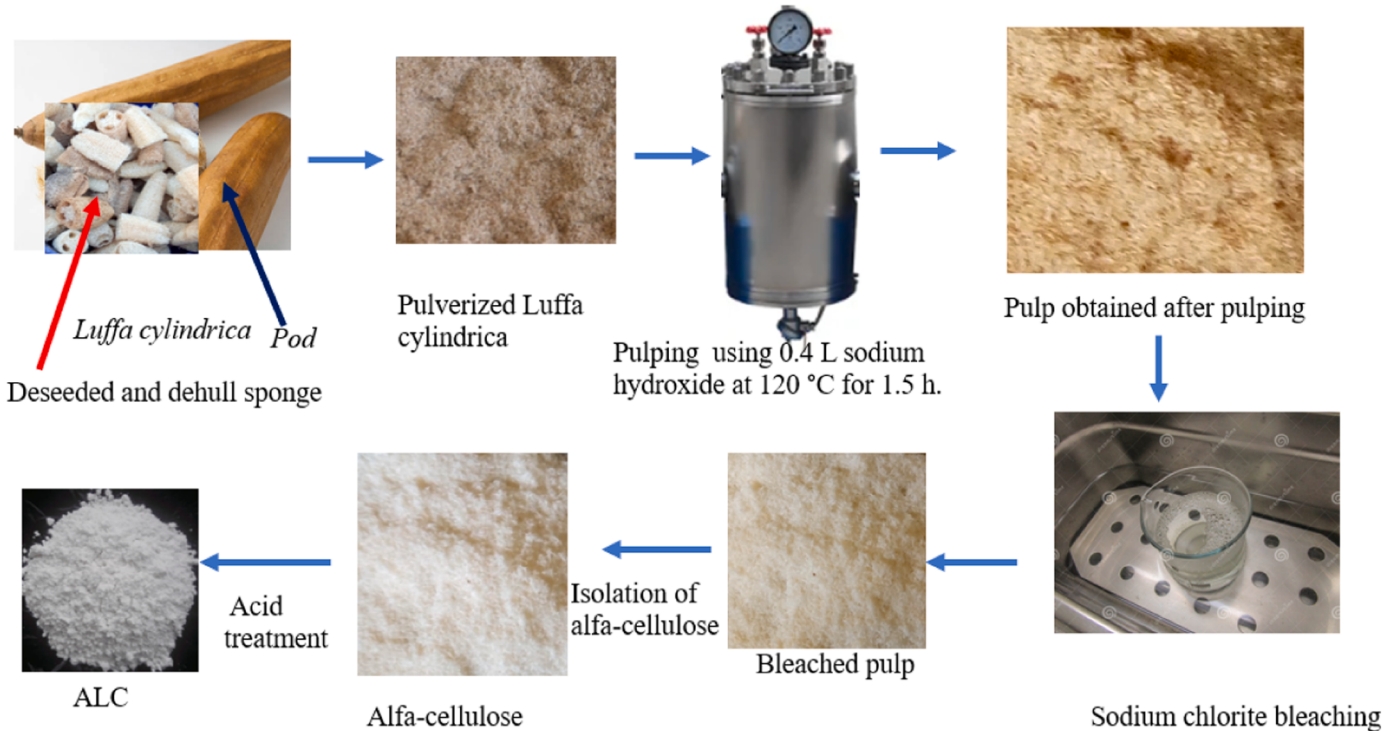


Fig. 1. Schematic diagram of ALC production.

(0.01 L, 30%) and stirring for 0.5 h. The resulting mixture was washed with HCl (0.5 L, 0.1 M) and de-ionized water (1 L) and centrifuged at 4000 rpm to obtain a gel-like substance which was oven-dried at 80 °C, labelled as graphene oxide (GO), and stored in a desiccator.

2.4. Preparation of bioplastic films

The bioplastic films with varying compositions of starch, ALC-cellulose, and GO (Table 1) were prepared following a slight modification of a method reported by our group [35]. Briefly, a suspension of cassava starch (5 g) in glycerin (2 mL) was added to distilled water (65 mL), and varying amounts of ALC-cellulose and GO were added depending on the target bioplastic film (Table 1). The mixture was heated at 70 °C with continuous stirring for 15 min. Subsequently, 50 mL of the resulting semi-solid was poured into a cast mould and left to set for 30 min, after which it was oven-dried at 75 °C for 4 h (Fig. 2). The dried sample was subsequently detached from the mould and stored in a desiccator at room temperature (27 °C) and 65% relative humidity. A control bioplastic sample (Film_0) was prepared using only starch.

2.5. Determination of physical properties of bioplastic films

Unless otherwise stated, the physical properties were determined in triplicates using 2 cm × 2 cm bioplastic films. The thickness d was measured at ten different points of the bioplastic films using a digital Vernier calliper, and the average value was recorded [29].

Table 1
Composition of bioplastic films.

Bioplastic film	Composition (%)		
	Starch	ALC-cellulose	GO
Film_0	100	0	0
$\text{Film}_{\text{cr}1}$	95	0	5
$\text{Film}_{\text{cr}2}$	92.5	0	7.5
$\text{Film}_{\text{cr}3}$	75	20	5
$\text{Film}_{\text{cr}4}$	72.5	20	7.5

The density, ρ was determined using the Eq. 1, [36]

$$\rho = \frac{M}{Ad}, \quad (1)$$

M is mass, A is total surface area, and d is thickness.

The percentage moisture content (%MC) was determined by Eq. 2, [32]

$$\% \text{MC} = \frac{W_1 - W_2}{W_1} \times 100, \quad (2)$$

W_1 is the weight of the bioplastic film before drying, and W_2 is the weight of the film after drying at 105 °C and 3 h.

The percentage opacity (%Op) was determined using the Eq. 3, [37]

$$\% \text{Op} = \frac{A_{600\text{nm}}}{d} \times 100, \quad (3)$$

$A_{600\text{nm}}$ is the absorbance of light ($\lambda = 600$ nm) measured using a U.V./Vis spectrophotometer (bioplastic was placed on the inner wall of a cuvette), and d is the thickness of the bioplastic film. A reference absorbance measurement using an empty cuvette was also undertaken.

The percentage swelling ability (% S.A.) was determined by Eq. 4, [33]

$$\% \text{SA} = \frac{W_1 - W_o}{W_1} \times 100, \quad (4)$$

where W_1 is the weight of the bioplastic film after soaking in de-ionized water (40 mL) for 24 h, and W_o is the weight of the film (dried at 105 °C for 3 h) before soaking.

The water absorption rate (W.A.C.) was determined by Eq. 5, [38]

$$\text{WAC} = \frac{\frac{W_f - W_d}{W_d} \times 100}{t}, \quad (5)$$

W_f is the weight of wet bioplastic film after soaking in water (30 mL) for time t , and W_d is the weight of film (dried at 105 °C) before soaking.

The percentage porosity (% φ) was determined using Eq. 6, [39]

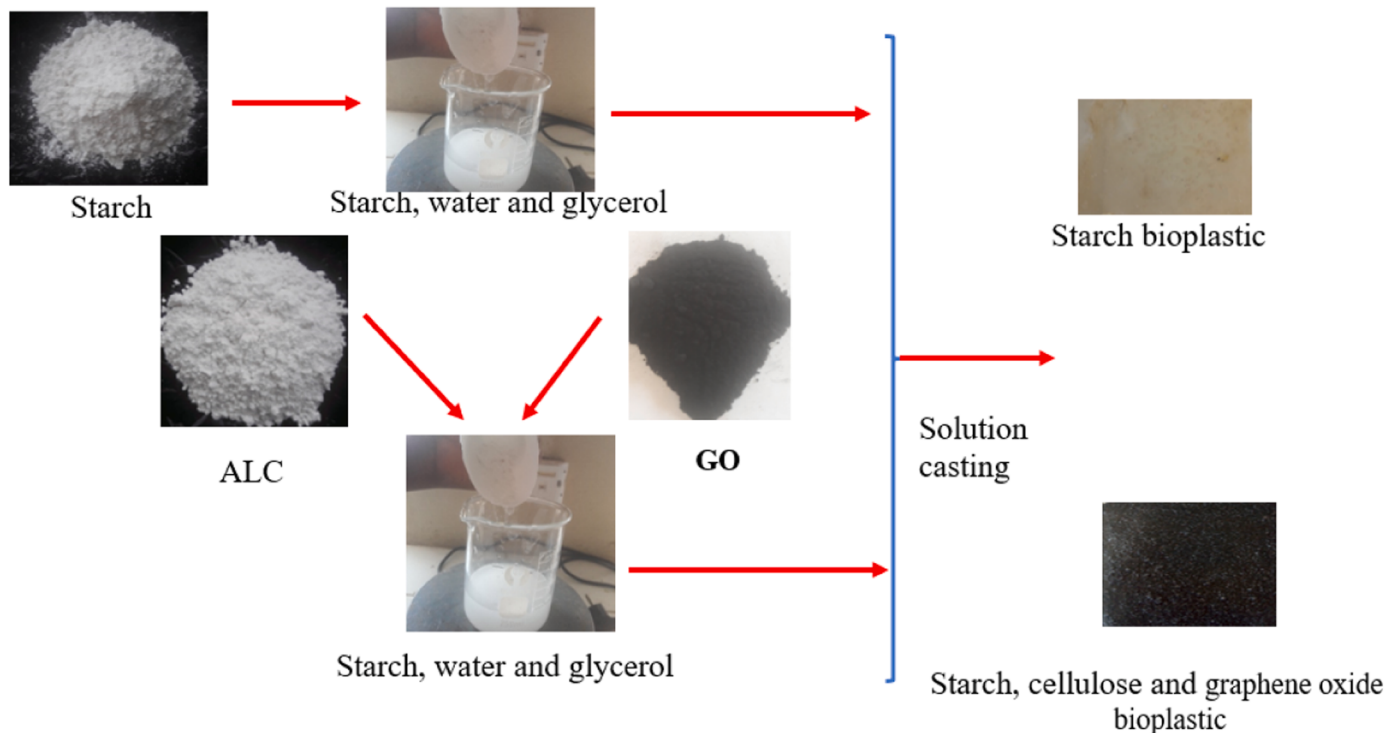


Fig. 2. Schematic diagram for the production of biofilm.

$$\% \varphi = \left[\frac{W_i - W_o}{\rho_{water}} \right] \times \frac{100}{V} \quad (6)$$

where W_i , W_o , ρ_{water} , and V are the weight of bioplastics in the wet state, dry state, water density, and bioplastic volume in the wet state.

The crystallinity index (CrI) was determined by Eq. 7, [40]

$$CI(\%) = \frac{\text{crystalline band areas}}{(\text{crystalline band areas} + \text{amorphous band area})} \times 100 \quad (7)$$

The crystalline and amorphous areas were determined by analysis of the XRD data.

2.6. Determination of mechanical properties of bioplastic films

The determination of the bioplastic films' mechanical properties, including tensile strength, elongation at break, and Young's modulus, was undertaken in triplicates using a testing machine fitted with a 50 K. N. cell load capacity and an extensometer of 0–50 nm. The loading was continuously measured by a load transducer (load cell) mounted between the specimen and the crosshead following the American Society for Testing and Materials guide (ASTM D 882-02) [41].

2.7. Determination of electrical properties of bioplastic films

The electrical properties, specifically dielectric constant and conductivity, were determined by adopting the method of Rani et al. [42]. Briefly, to determine the dielectric constant, a bioplastic film of known diameter and thickness was placed between two circular aluminium blocks and inserted into a cylindrical plastic pipe for easy handling. The capacitance (C) of the bioplastic film was then measured using a range from 0 to 100 μF instead of 100 pF. The result obtained was used for the computation of the dielectric constant by Eq. 8,

$$C = \frac{\epsilon_0 \epsilon_r A}{d} \quad (8)$$

Where ϵ_0 is the permittivity of free space, ϵ_r is the dielectric constant,

A is the cross-sectional area of the sample, and d is the thickness of the sample.

The electrical conductivity was determined at room temperature using Eq. 9,

$$\delta = \frac{d}{RA} \quad (9)$$

d , R and A are the bioplastic film's thickness, resistance, and surface area. The thickness and area of the bioplastic films were determined as previously described.

The resistance was determined using Eq. 10,

$$R = \frac{V}{I} \quad (10)$$

where I is the current across a voltage (V) applied to the material.

2.8. Characterization

The LC-cellulose and ALC-cellulose, graphite, and GO samples were identified utilizing X-ray diffraction (XRD), which was collected on a Panalytical Empyrean X-ray diffractometer employing a Co $\text{K}\alpha$ radiation ($\lambda = 1.790955 \text{ \AA}$) at 40 kV and 40 mA and a scan duration for each sample was 90 min. The functional groups were identified using Fourier transform infrared spectroscopy (FTIR), which was recorded on a Bruker Alpha Platinum-Attenuated Total Reflectance I.R. spectrometer in the 4000–400 cm^{-1} range using neat samples of the materials. The Raman spectra were measured on a Renishaw InVia Raman microscope with a HeNe laser source (20 mW) and excitation at a wavelength of 633 nm. The surface morphology of the materials was revealed through scanning electron microscopy (SEM), undertaken using LEO 1450 SEM by attaching the samples on a brass stub and coating with gold before the SEM imaging. Further information on the surface morphology of the samples was obtained after transmission electron microscopy (TEM) imaging, which was undertaken on a JOEL 2100+ machine operating an acceleration voltage of 200 kV from samples prepared by dissolution in ethanol and deposition (one drop) on a copper EM grid. The sizing of the

materials was determined by analysis of the TEM images using the ImageJ software. Thermal stability was investigated using thermogravimetric analysis (TGA), which was undertaken using a Mettler Toledo DSC1-STAR at a scan rate of 10 °C/min on a sample placed inside 70 µL alumina pans under a nitrogen atmosphere from 25–900 °C. The bio-plastic film's absorption was measured using a Schimadzu model 1800 UV/Visible spectrophotometer. Volumetric capacitance was measured using the Matech MS8268E standard capacitance meter. Electrical conductivity was determined using a Keithley 199 system 199 DMM/scanner multimeter, which automatically calculated resistance in a four-point probe configuration.

3. Results and discussion

3.1. XRD

The X-ray diffractograms of the LC-cellulose and ALC-cellulose samples presented in Fig. 3a are identical to those reported for the cellulose materials in the literature [43]. The ALC-cellulose's crystallinity index was 62% higher than the 52% of the LC-cellulose sample. The higher crystallinity index indicates that the acid removed some of the amorphous and non-cellulose portions of the LC-cellulose. The X-ray diffractograms of graphite flakes and graphene oxide (GO) presented in Fig. 3b were used to probe their crystal phase and to determine the interlayer spacing. The waste dry cell battery-sourced graphite shows the typical sharp diffraction peak at $2\theta = 30.79^\circ$, suggesting the existence of a well-defined layer with a *d*-spacing of 0.29 nm (FWHM = 0.588) [44]. The GO prepared by the oxidation of the graphite had three major peaks, with the characteristic GO peak appearing at $2\theta = 11.59^\circ$ with an increase in the interlayer *d*-spacing to 0.76 nm (FWHM = 0.285) from 0.29 nm (for graphite). The presence of the peaks and the increase in the interlayer *d*-spacing suggest an oxidized product with the potential introduction of hydroxyl, epoxy, and carboxyl groups causing intercalation of water molecules with resultant distance increment between the layers [45]. Finally, the 2θ value of 31.50° has been attributed to well-graphitized two-dimensional structures made of GO [46].

3.2. FTIR

The FTIR spectra of the LC-cellulose and the ALC-cellulose samples are presented in Fig. 4a. In both spectra, broadbands at 3317 cm^{-1} , medium peaks at 2890 cm^{-1} , and sharp peaks at 1020 cm^{-1} were observed, corresponding to the hydroxyl O-H, the saturated C-H and the aliphatic ether C-O stretches, respectively. The observed peaks are consistent with cellulose peaks found in the literature [47]. The FTIR spectrum (4b) of the waste dry cell battery-derived graphite contains a peak at 1795 cm^{-1} representative of the carboxylic C=O [13]. The observed weak bands may be attributed to the various compounds

(manganese dioxide, zinc chloride, or ammonium chloride) associated with the graphite in the waste dry cell battery. In contrast, the spectrum of the GO contains broadband at 3195 cm^{-1} , weak broadband at 2664 cm^{-1} , a sharp peak at 1538 cm^{-1} , and a broad peak at 1031 cm^{-1} , corresponding to the hydroxyl O-H stretch, saturated C-H stretch, cyclic alkene C=C stretch and aliphatic ether C-O stretch respectively [48,49]. The observed peaks indicate the successful Preparation of GO from the battery-derived graphite.

3.3. Raman

The Raman spectra of the waste dry cell battery-derived graphite and the GO, as presented in Fig. 5, indicate the presence of D and G bands, except for an additional 2D band. The sp^2 carbon atoms band observed at 1584 cm^{-1} corresponding to the G band indicates the graphite nature of the material [50]. Further, the D band was observed at 1356 cm^{-1} and the 2D band at 2707 cm^{-1} , attributed to the second-order double resonant process between non-equivalent K points observed in the Brillouin zone of graphene [51]. The presence of manganese oxide, zinc chloride and ammonium chloride in the spent Leclanche zinc-carbon graphite rod could have caused the observation of the D band in the graphite. After the chemical treatment of the graphite, the D and G band positions were noticed to have changed. The D band reduced from 1356 cm^{-1} to 1349 cm^{-1} ; this could be due to the structural defect of the graphite by the attachment of the oxygen functional group, causing sp^3 defects in the sp^2 lattice of the graphite [50]. The shift in the G band position from 1584 cm^{-1} (graphite) to 1596 cm^{-1} (GO) corroborates the earlier claim of the distortion of the sp^2 lattice of the graphite because the shift has been proposed to be due to the destruction of symmetry because of shrinking of the in-plane sp^2 domains caused by the oxidation of the graphite [52]. The intensity ratios (I_D/I_G) for graphite and GO were found to be 0.86 and 0.84, respectively. Similar observations have also been reported in the literature [53].

3.4. SEM

The S.E.M. micrographs of the LC-cellulose and ALC-cellulose are presented in Fig. 6a and b, respectively. The micrograph of the ALC-cellulose differs from that of the precursor LC-cellulose. While the micrograph of LC-cellulose contains bundles of fibres sitting on a sheet of material suspected to be residual lignin and other non-cellulosic materials, the micrograph of ALC-cellulose shows an isolated strand of fibre without the lignin material. The difference in structure could be attributed to the acid hydrolysis treatment that helped remove the non-cellulosic materials. The SEM. micrographs of the graphite and GO are presented in Fig. 6c and d, respectively. Graphite and GO present different morphological structures. The starting material (graphite rod)

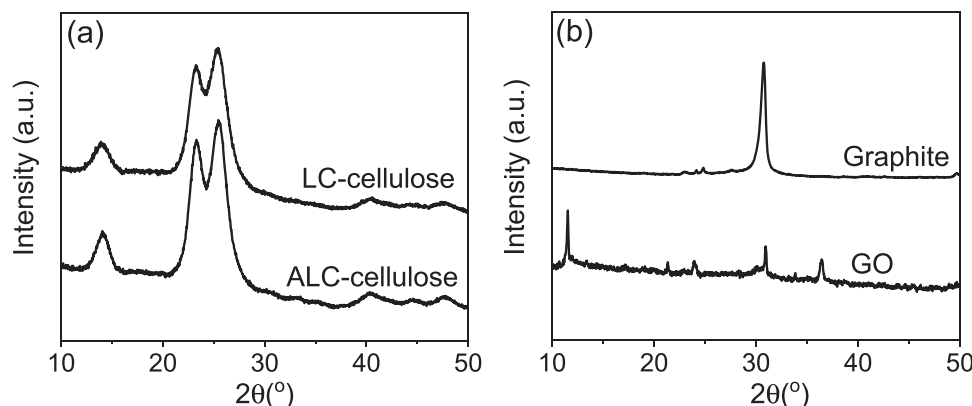


Fig. 3. X-ray diffractograms of (a) LC-cellulose and ALC-cellulose, (b) graphite and GO.

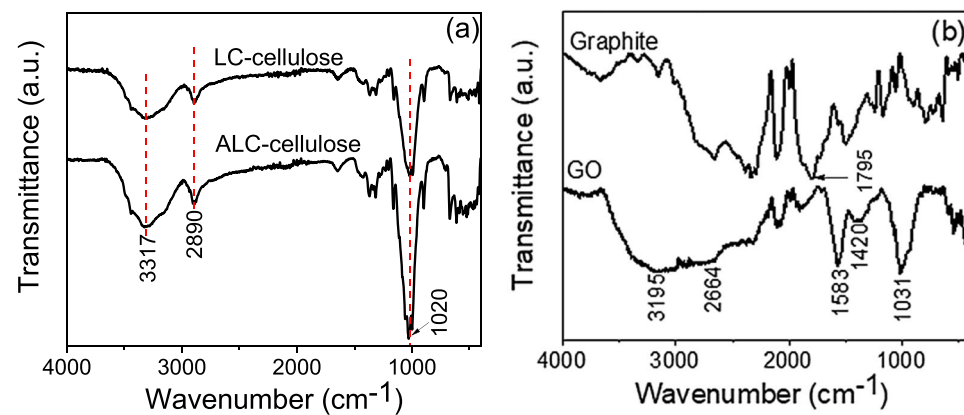


Fig. 4. FTIR spectra of (a) LC-cellulose, ALC-cellulose, (b) graphite (from the rod in spent dry cell zinc-carbon battery), and graphene oxide (GO).

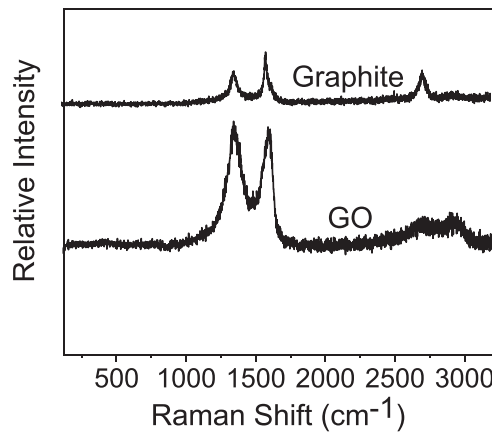


Fig. 5. Raman spectra of graphite and graphene oxide (G.O.).

appears as amorphous aggregated flakes. In contrast, the GO sample appears as a flat rectangular rod-like material, indicating oxidation of the graphite to GO [54]. The difference in structures may be due to the removal of the non-graphitic materials by the acid treatment, leaving behind the highly ordered graphene oxide.

3.5. TGA

The TGA thermograms for LC-cellulose and ALC-cellulose are presented in Fig. 7a. Both samples show identical step weight loss patterns but different actual percentage weight losses, indicating their compositions' differences. The weight losses of 7.1% for cellulose and 4.0% for ALC-cellulose at 105 °C were attributed to moisture loss [55]. The higher percentage of moisture content in the cellulose sample could be a result of the presence of a higher percentage of undissolved lignin, hemicellulose, and other non-cellulose, most of which are amorphous and have the tendency to retain moisture better than ALC-cellulose [56]. The weight losses of 72.4 and 79.7% by LC-cellulose and ALC-cellulose, respectively, between 240 and 398 °C were attributed to the degradation of cellulose in both samples. Also, for this second step loss, both samples appear to have identical onset temperatures, indicating that LC-cellulose and ALC-cellulose have identical stability. The TGA thermograms for the graphite and GO are presented in Fig. 7b. Both samples were observed to demonstrate different step loss patterns, indicating the difference in their compositions. The weight loss of only 3.3% between 187 and 347 °C observed for graphite was attributed to the combustion of non-graphitic components of the sample, considering that the graphite sample was made up of various compounds (such as binder) in the waste dry cell battery starting material. The GO sample was observed to show

three sets of weight losses. The weight losses of 8% (between 25 °C and 20 °C), 13% (between 120 °C and 220 °C), and 18% (between 220 and 900 °C correspond to loss of moisture, decomposition of oxygen functional groups, and reduction of the GO sample respectively [17,57,58].

3.6. T.E.M

The transmission electron micrographs of the LC-cellulose, ALC-cellulose, graphite and GO samples are displayed in Fig. 8. While the LC-cellulose and ALC-cellulose samples appear to show similar morphologies, the average fibre diameter of the ALC-cellulose (44.7 nm) was noticed to be lesser than that of the LC-cellulose (99.7 nm), highlighting the difference in the two materials. The graphite and GO all appear as sheet-like semi-transparent materials (Fig. 8). The graphite sample also revealed a conglomeration of particles of various shapes and sizes. The GO insert image revealed a stacked flake-like structure and was smoothly arranged with an average diameter of 54.7 nm. The high-resolution transmission electron micrograph (HRTEM) provides more insight into the morphology of the materials (Fig. 9). The HRTEM of the graphite indicated a fragile, flat material, and that of GO revealed the flake-like pile structure. The dark spot of the GO has been suggested to be the effect of the presence of sp³ hybridized carbon atom-bearing hydroxyl groups [59].

3.7. Physical properties of bioplastic film

3.7.1. Thickness

Determining bioplastic film thickness is essential as it influences other properties, such as opacity. A linear relationship was observed between the thickness of the bioplastic films and the amount of GO and ALC-cellulose added, with the bioplastic films - Film_{cr3} and Film_{cr4} containing ALC-cellulose showing the highest thickness (Fig. 10a). Film_o had the lowest value of 0.21 mm, while Film_{cr4} had the highest value of 0.48 mm. The increase in the film thickness might be due to the incorporation of GO and fibres. Similar behaviour was reported by Sanjay et al. [60], where the thicknesses of a set of bioplastics prepared increased with increased quantities of filler materials added. In addition to the type of filler materials, the method of preparation and the casting mould used could also influence the thickness of the bioplastic film.

3.7.2. Density

The density of carbon-based materials greatly influences the volumetric and gravimetric capacitances [61]. A linear relationship was investigated between the densities of the bioplastic films and the amount of filler materials (GO and ALC-cellulose) used. It was noticed that the density of the bioplastic films increased from (1.31±0.01) g/cm³ for Film_o to (1.44±0.02) g/cm³ for Film_{cr4}, and this follows the same trend

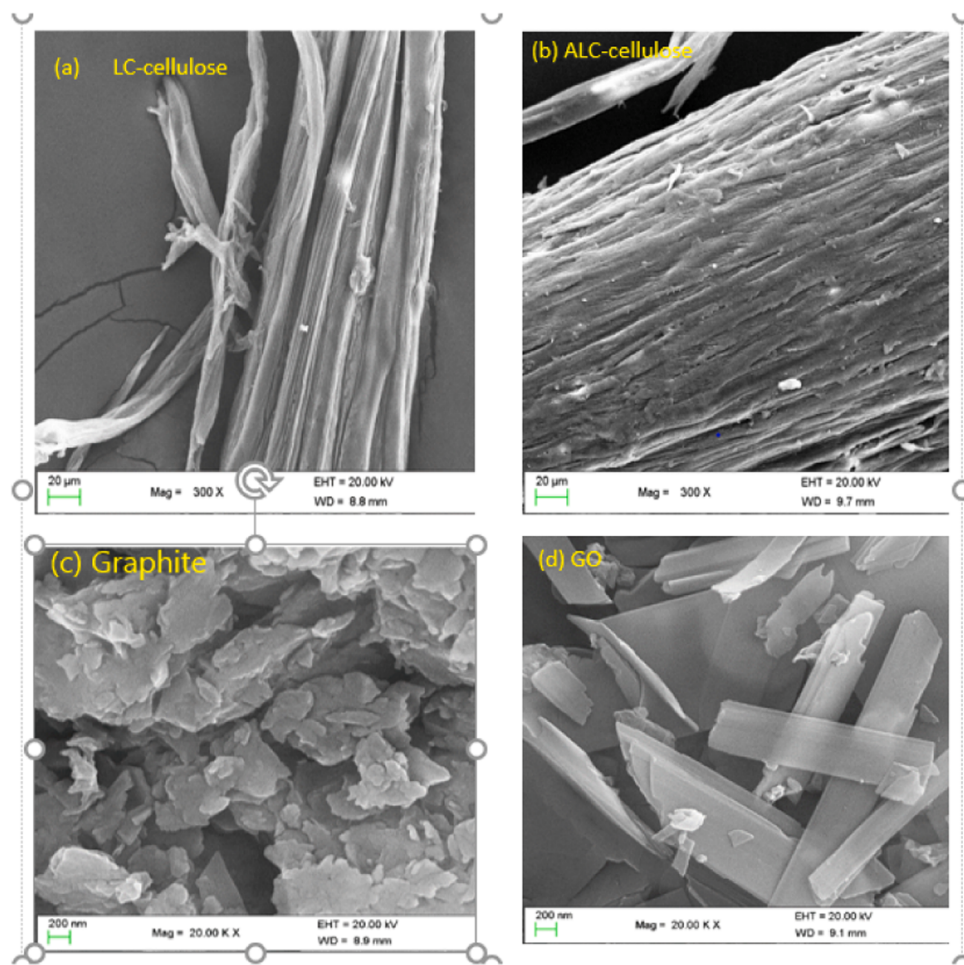


Fig. 6. S.E.M. micrographs of (a) LC-cellulose, (b) ALC-cellulose, (c) graphite, and (d) graphene oxide (GO).

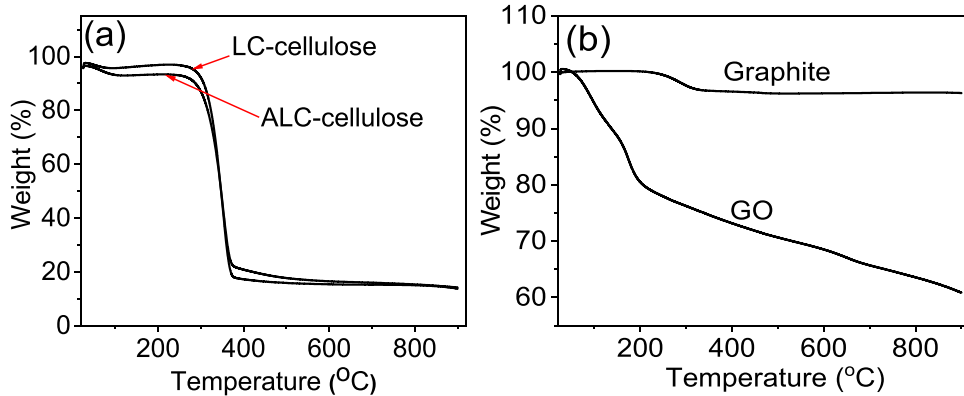


Fig. 7. TGA thermograms of (a) LC-cellulose and ALC-cellulose, (b) graphite, and graphene (G.O.).

as for the thickness study (Fig. 10b). The density increase could be linked to the increase in the mass of the added solid materials used in the bioplastic preparation, as was also observed by Maulida et al. [62]. In practical terms, it is expected that the volumetric capacitance of the Film_{cr4} will be the highest of all the bioplastics prepared since it has the highest density. On the other hand, the Film_{cr4} will have the lowest gravimetric capacitance of the bioplastic materials since the high density reduces the ion-accessible surface area [61].

3.7.3. Moisture content

The moisture content was found to be on a reducing trend, from 8.4%

(Film₀) to 3.5% of (Film_{cr4}), as the concentration of the GO and ALC-cellulose used increased with ALC-cellulose accounting for the significant reduction in moisture content (Fig. 10c). Film_{r1} containing the GO filler only (5% w/w) has a moisture content that is 3% lesser than that of the Film₀ without GO. Furthermore, an increase in the GO content of the bioplastic three-fold in the Preparation of Film_{r2} caused a reduction of the moisture content of Film_{r2} by approximately 4% compared to Film₀. These could be explained by the increment in film solid particles by the GO. However, on comparing Film_{r2} and Film_{cr4} which differs only by the 20% mass of ALC-cellulose filler, the moisture content of the Film_{cr4} is about 57% lesser than that of Film_{r2}. Suppose moisture content

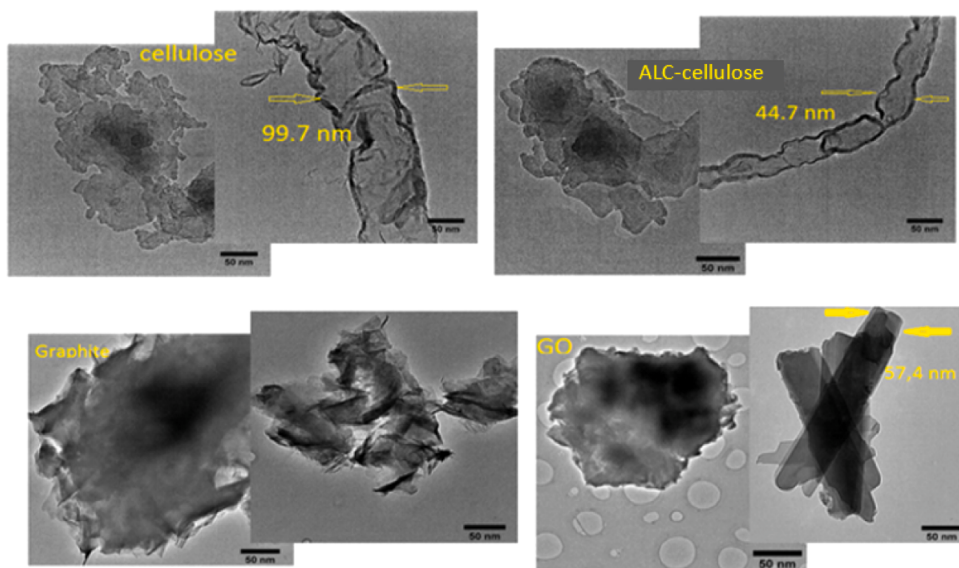


Fig. 8. TEM micrographs of LC-cellulose, ALC-cellulose, graphite, and graphene (GO).

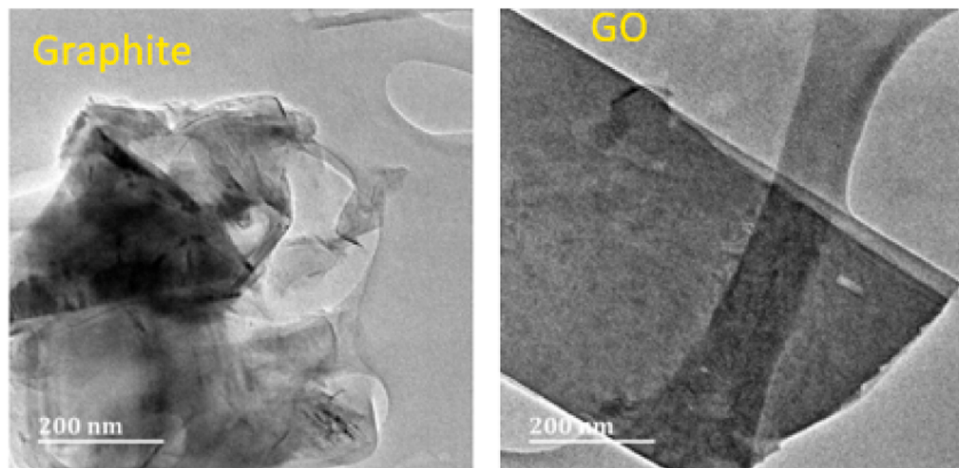


Fig. 9. High-resolution TEM micrographs of graphite and graphene oxide (GO).

reduction from one bioplastic film to another is compared per % mass of filler added. In that case, roughly 0.55% and 3% reduction in moisture content are achieved per %mass of GO and ALC-cellulose used, respectively. From the percentage moisture reduction, GO contributes less to the reduction in moisture content compared to ALC-cellulose, and this could be attributed to the higher water absorption capacity of GO compared to the ALC-cellulose due to the presence of carboxyl, epoxy, and hydroxyl oxygen atoms in GO which could form more hydrogen bonds with water than only hydroxyl oxygen atoms in ALC-cellulose. Another plausible reason is that GO is less crystalline than ALC-cellulose. The moisture content of the bioplastic films in this work was lower than 13.21 – 17.59% for corn starch bioplastic film with different percentages of essential oils [63], 15.3 – 24.8% for tree cassava starch biodegradable films [64] and 9.30 – 11.41% for *Dioscorea dumetorum* starch films with added dialdehyde starch solution [35]. The lower moisture contents in our study may be attributed to the use of the ALC-cellulose and GO, as explained above.

3.7.4. Opacity

A material's opacity is a vital property usually determined in material science as it may dictate the applications to which the material may be put. For instance, materials with low opacity (in other words, high

optical transparency) could be employed as biophotonic materials in biomedical applications [65]. It was observed that the opacity of the bioplastic films followed the same trend as the thickness as it increased with an increase in the number of filler materials (GO and ALC-cellulose), and the GO contributed more to the opacities of the bioplastic films than ALC-cellulose (Fig. 10d). The use of GO (5% w/w) conferred Film_{r1} with an opacity roughly 65% greater than that of Film_o. When the amount of GO added was increased by 2.5% w/w to get the Film_{r2}, the Film_{r2} displayed an opacity of 20% higher than that of Film_{r1}. A comparison of the opacities of Film_{r2} and Film_{cr4} containing 0 and 20% w/w of ALC-cellulose, respectively, reveals that the opacity of Film_{cr4} is approximately 20% higher than that of Film_{cr2}. Considering that the use of GO (5% w/w) afforded a 65% increase in opacity, while the use of ALC-cellulose (20% w/w) afforded only a 20% increase in opacity as discussed above, indicates that GO may be primarily responsible for the observed opacities in the bioplastic films and this is because GO deepens the colour of the bioplastic film, but cellulose does not. These results indicate that GO is a good filler for materials required for light-blocking applications. At the same time, ALC-cellulose is a good filler material for bioplastics required for biophotonic materials.

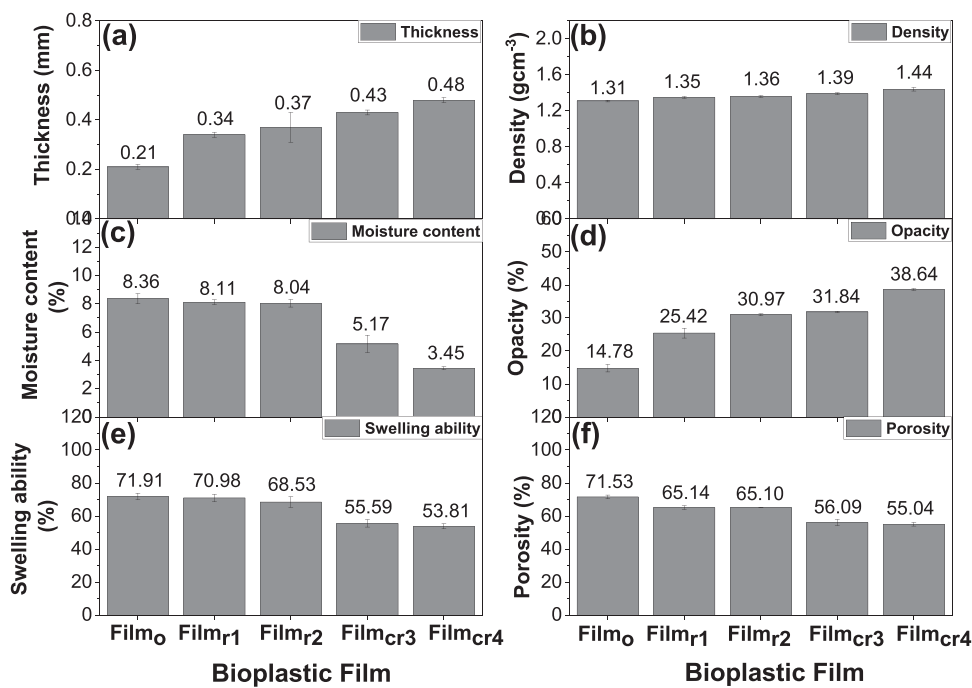


Fig. 10. (a) Density, (b) thickness, (c) moisture content, (d) opacity, (e) swelling ability, and (f) porosity of bioplastic films.

3.7.5. Swelling ability

The percentage swelling abilities of the bioplastic films are presented in Fig. 10e. Film_o has the highest swelling ability of 71.9%, attributed to the hydrophilicity of the starch. Film_{r1} and Film_{r2} recorded swelling abilities of 71.0% and 68.5%, respectively, which are slightly lower than that of Film_o, indicating that the use of GO did not significantly reduce the swelling abilities of Film_{r1} and Film_{r2}, probably because of the presence of carboxyl, epoxy, and hydroxyl oxygen atoms, which are hydrophilic. Additionally, the minimal reduction in swelling abilities observed in Film_{r1} and Film_{r2} could be attributed to the blockage of available pores of those bioplastics by the GO, leading to reduced film and water interaction, which could have prevented bioplastics swelling. Film_{cr3} and Film_{cr4} were observed to show swelling abilities of 55.6% and 53.8% respectively which are significantly lower than those of Film_o, Film_{r1}, and Film_{r2}, demonstrating that the incorporation of ALC-cellulose imparts a significant reduction in swelling abilities, perhaps owing to the higher crystalline nature of ALC-cellulose compared to GO. A similar observation was reported by Nugroho et al. [66] where it was noticed that the swelling ability of starch reduced after reinforcement with a cellulose filler. Overall, the results show cellulose filler was more effective in reducing the bioplastic swelling than GO.

3.7.6. Porosity

Porosity determination is essential as it influences the conductive property of a bioplastic film. Bioplastic films for conductive applications should have low porosities to prevent pores that could interfere with the flow of electrons. This study observed that adding the filler materials - GO and ALC-cellulose- lowered the bioplastic film sample's porosity. The bioplastic film without any reinforcement (Film_o) has the highest porosity of 71.5%, while the bioplastic films with GO and ALC-cellulose reinforcements had lower porosities (Fig. 10f). It was also observed that bioplastic films containing ALC-cellulose fillers showed much lower porosities than films containing only GO. (Fig. 10f). Film_{cr3} and Film_{cr4} containing ALC-cellulose and GO had porosities of $(56.09 \pm 1.88)\%$ and $(55.04 \pm 1.13)\%$, respectively, which are lower than the $(65.14 \pm 1.12)\%$ and $(65.10 \pm 0.10)\%$ for Film_{r1} and Film_{r2} respectively containing only GO and this could be linked to the tighter packing of the ALC-cellulose fibre than that of the GO particles. The porosity results show that Film_{cr4}

will be most suited for use in electronic devices, which was supported by Ma et al.'s findings [67].

3.7.7. Water absorption rate

The ability of bioplastic to resist water absorption and slow transportation between its matrix can be studied through the water absorption rate (WAR). The ability of bioplastic to retard water absorption is a good indication of the durability of the bioplastic in a high-humidity environment. The highest WAR of 0.24s^{-1} (obtained by dividing the 92% water absorbed by the 380 seconds it takes to absorb water) was observed for Film_o (Fig. 11), which is attributed to the hydrophilicity of the starch in Film_o. Film_{r1} and Film_{r2}, with only 5 and 7.5% GO content, respectively, show WAR values (Film_{r1}: 0.24s^{-1} , Film_{r2}: 0.23s^{-1}) like that of Film_o within experimental error, proving that the starch component of these bioplastics is responsible for their high WAR. The lowest WAR value of 0.20s^{-1} was observed for Film_{cr3} attributed to the increased water impermeability property introduced by the crystalline nature of the ALC-cellulose filler added [68]. Film_{cr4}, with the same percentage composition of ALC-cellulose as Film_{cr3}, showed a WAR value of 0.21s^{-1} like that of Film_{cr3} within experimental error, confirming that the ALC-cellulose filler is responsible for the lowering of the

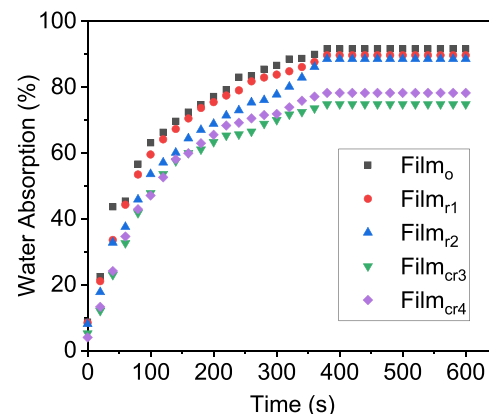


Fig. 11. Water absorption kinetics of the bioplastic film.

water absorption rate of these bioplastic films. Other researchers reported similar results for composites of polymer blends, cellulose fibres [69], and hemicelluloses added to a starch matrix [70]. These results showed that fortifying starch-based bioplastic films with ALC-cellulose reduces the water absorption rate.

3.7.8. Bioplastic TGA

TGA measurements of the bioplastic films were undertaken to determine the thermal stabilities. It was noticed that the step losses for all bioplastic films are similar, perhaps due to the small number of filler materials used (Fig. 12). Also, the type and amount of filler material added to the bioplastic film influenced the thermal stabilities, and the GO contributed more to the thermal stability than the ALC-cellulose. For example, the Film_{r1} showed similar thermal stability as the control bioplastic film – Film_o and this could be credited to the small amount of the GO (5% w/w) used with both bioplastic films losing roughly 75% of the weights over the entire temperature range. However, on increasing the GO amount to 7.5% in Film_{r1}, slightly better thermal stability was observed than the Film_o as Film_{r1} lost 72% of its initial weight. In comparison, Film_o lost 75% in the same temperature range. On the other hand, the Film_{cr3} and the Film_{cr4} containing ALC-cellulose display lower thermal stabilities than the control bioplastic film (Film_o) as both the Film_{cr3} and the Film_{cr4} lose a more significant amount of the initial weight (80%) compared to Film_o which lost only 75%. The higher thermal stability imparted by GO compared to ALC-cellulose could be rationalized primarily by the higher carbon-to-oxygen ratios in GO than in cellulose, as a high amount of oxygen atoms facilitates decomposition [71]. Film_{r1}, Film_{r2}, and Film_{cr3} show identical step loss patterns to the control bioplastic film (Film_o) except for Film_{cr4}, attributed to the poor thermal stability of ALC-cellulose (Fig. 12). Overall, the results have demonstrated that an increase in the composition of GO filler material could increase the thermal stability of the starch-based bioplastic film.

3.8. Mechanical properties

3.8.1. Tensile strength

The tensile strength of a material is inversely correlated with porosity [72]. Low porosity materials have high tensile strength and vice versa. Therefore, following the porosities discussed earlier, it is expected that the trend of the tensile strengths of the bioplastics will be in the order Film_o < Film_{r1} < Film_{r2} < Film_{cr3} < Film_{cr4}. As expected, the average tensile strengths increase from Film_o to Film_{cr4} (Fig. 13a). ALC-cellulose contributed more to the increase in tensile strength than GO. For instance, adding GO increased the tensile strength in Film_{r1} by 0.08 compared to Film_o. However, adding ALC-cellulose increased the tensile strength in Film_{cr3} by 0.24 compared to Film_{r1}. The higher influence of ALC-cellulose than GO on tensile strength could be attributed to the creation of intermolecular hydrogen bonding between the starch

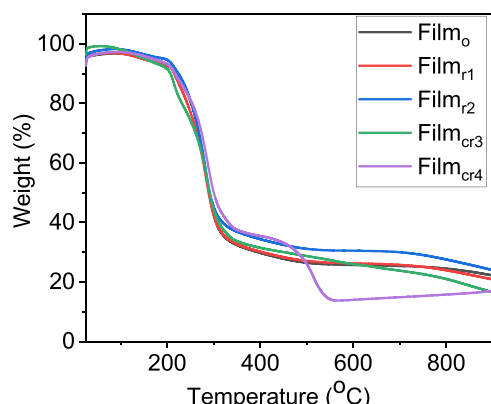


Fig. 12. TGA thermograms of bioplastic films.

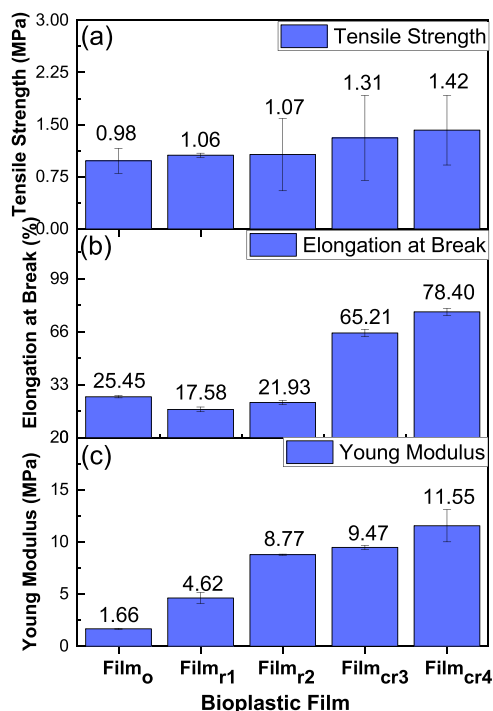


Fig. 13. (a) Tensile strength, (b) Elongation at break, and (c) Young modulus of the bioplastic films.

base and ALC-cellulose [73]. The tensile strengths obtained here are lower than those reported by Santana et al. [73], where glycerol-fortified starch-based bioplastic films were prepared, and this difference could be linked to the different types of starch samples and filler materials used.

3.8.2. Elongation at break

The elongation at break (EB), or fracture strain, represents the length ratio increased by stretching after the material is broken to the initial length. It is worth pointing out that the elongation at break investigation revealed two observations. First, from Fig. 13b, the bioplastic films containing only the GO filler (Film_{r1} and Film_{r2}) display lower E.B. than the control bioplastic film (Film_o), indicating that the GO interacts with the starch to induce brittleness in the film, and this may be because GO has a rigid sheet-like structure with inelastic sp³ carbon-carbon bonds [74]. Similar results were observed by Ekebafe and coworkers [75], who found out that the EB of natural/GO composite were lower compared to the composites without the GO [75]. Though an increase in the GO content in Film_{r2} afforded a slight increase in EB compared to Film_{r1}, the reason remains unclear. Secondly, the bioplastic films containing the ALC-cellulose fillers (Film_{cr3} and Film_{cr4}) demonstrated higher EB than all the films without the ALC-cellulose (Film_o, Film_{r1} and Film_{r2}), showing that ALC-cellulose confers ductility to the film, ascribed to the linear chain-like structure of cellulose which could have helped the film orientate in the same direction as the applied load [76]. Arjmandi's group reported similar findings where the cellulose nanowhiskers content of some polylactic acid/cellulose nanowhiskers composite occasioned a corresponding increase in the E.B. [77].

3.8.3. Young's Modulus

Young's modulus increased with the percentage composition of fillers (Fig. 13c). Film_{r1} and Film_{r2} containing only the GO filler (Table 1) provided a 3- and 5-fold increase, respectively, in Young's modulus compared to the control bioplastic film – Film_o, and this could be traced to the stiffness effect of the GO [77]. This result is like that reported by Ekebafe et al. [75]. Furthermore, Film_{cr3} and Film_{cr4}

containing both the GO and ALC-cellulose fillers displayed even higher Young's modulus than Film_{r1} and Film_{r2}, indicative of the synergistic stiffness effect of the fillers. However, a higher value of modulus was observed in Film_{cr4} than that of Film_{cr3}, probably due to a higher amount of added GO. Similar observation was reported by Veyra's group [78].

3.9. Electrical properties

3.9.1. Dielectric constant

The electrical properties of the bioplastic films were investigated at room temperature, and the results are presented in Fig. 14. The control bioplastic sample (Film_o) showed a dielectric constant of 50.33, attributed to the buildup of charges at the interfaces of the starch amylose (crystalline region) and amylopectin (amorphous) because of the difference in their conductivities [79]. The dielectric constant of the bioplastic films increased with an increasing amount of GO and ALC-cellulose added from 50.33 for Film_o (with 0% GO w/w) to 1057.13 for Film_{r1} (with 5% GO) and from 693.96 for Film_{r2} (with 0% ALC-cellulose) to 6965.22 for Film_{cr3} (with 20% ALC-cellulose) respectively. The increase in the dielectric constant could be attributed to the increase in the buildup of charges at the interfaces of heterogeneous macroscopic components of the bioplastic films [80]. The reduction in the dielectric constant to 3033.73 for Film_{cr4} from 6965.22 Film_{cr3} might be because that additional GO added reduced interfacial and space charge polarization.

3.9.2. Electrical conductivity

The electrical conductivity of the bioplastic films is presented in Fig. 14b. The result shows that the type and amount of filler material influenced the direct current conductivity of the bioplastic films. The neat bioplastic Film_o containing 100% starch has the most minor conductivity, 3.6×10^{-3} S/m, attributed to the hydrogen bond between starch and glycerin [81]. By the replacement of 5% of the starch bioplastic with GO in Film_{r1} (starch: 95 and GO: 5% w/w) a conductivity of 10.9×10^{-3} S/m which is three times that of the control bioplastic – Film_o. An increase in the GO content to 7.5% in Film_{r2} (starch: 92.5% and GO: 7.5%) resulted in higher conductivity of 12.3×10^{-3} S/m, nearly four times that of the control bioplastic. The increase in conductivity afforded by the addition of GO in Film_{r1} and Film_{r2} may be due to delocalized electrons in the unsaturated sp² carbons, which were unoxidized during GO preparation as evidenced in the Raman spectra as well as the uniform dispersity of the GO filler [82]. Film_{cr3} containing not only GO (5% w/w) but also ALC-cellulose (20% w/w) showed an even higher conductivity of 14.7×10^{-3} S/m compared to Film_{r2}, also attributed to delocalized electrons in the unsaturated sp² carbons and uniform dispersion of the GO and ALC-cellulose in the bioplastic films. However, Film_{cr4}, with the same ALC-cellulose but higher GO content compared to Film_{cr3}, demonstrated a lower conductivity of 7.4×10^{-3} S/m than that observed for Film_{cr3}. The reduction in conductivity of

Film_{cr4} could be due to the reduced dispersity of the GO filler. Overall, the addition of the GO afforded improvement in the electrical conductivities of the bioplastic films.

4. Conclusion

Two fillers, acid-treated cellulose and graphene oxide, were prepared from *Luffa cylindrica L.* biomass and waste dry cell battery graphite rod, respectively. The fillers were used as reinforcement and electrically conductive materials to prepare starch-based bioplastics. The results of the physicochemical properties of the products revealed an improved properties trend. The density of the bioplastic films increased from 1.31 g/cm^3 for Film_o to 1.44 g/cm^3 for Film_{cr4}. The opacity of bioplastic without any additive Film_o was 14.78%, which increased to 38.64% for Film_{cr4}; on the other hand, the moisture content of the films experienced a reducing effect, Film_o recorded 8.36%, but Film_{cr4}, with the highest amount of fillers, recorded 3.45%. The fillers also influenced the mechanical properties of the films. The Film_o had a tensile strength of 0.98 MPa, while those with fillers had higher values with the highest being 1.42 MPa for Film_{cr4}. Thermogravimetry analysis of those bioplastic revealed that GO impacted better stability than the ALC-cellulose. The results showed that a synergic effect between the fillers caused an increase in the conductivity of the bioplastics. The neat bioplastic Film_o has the least conductivity of 3.6×10^{-3} S/m, Film_{r1} has 10.9×10^{-3} S/m, Film_{r2} recorded 12.3×10^{-3} S/m, while Film_{cr3} has 14.7×10^{-3} S/m 7.4×10^{-3} S/m. However, Film_{cr4}, with the same ALC-cellulose but higher GO content compared to Film_{cr3}, demonstrated a lower conductivity of 7.4×10^{-3} S/m than that observed for Film_{cr3}. The control bioplastic sample (Film_o) recorded a dielectric constant of 50.33. However, there was an increase in the dielectric constant of the bioplastic films when the two fillers were present in the bioplastic. Film_{r1} has 105.7, which increased to 693.96 for Film_{r2}. The improvement in physical and mechanical properties was mainly due to acid-treated cellulose rather than graphene oxide. Finally, higher dielectric constant and electrical conductivity were obtained with bioplastic films containing both acid-treated cellulose and graphene oxide than those with only one type of these fillers. The research has demonstrated the potential of discarded battery rod graphite and waste *Luffa cylindrica L* as viable secondary raw materials.

Declaration of Competing Interest

The authors declare no conflict of interest.

Data availability

No data was used for the research described in the article.

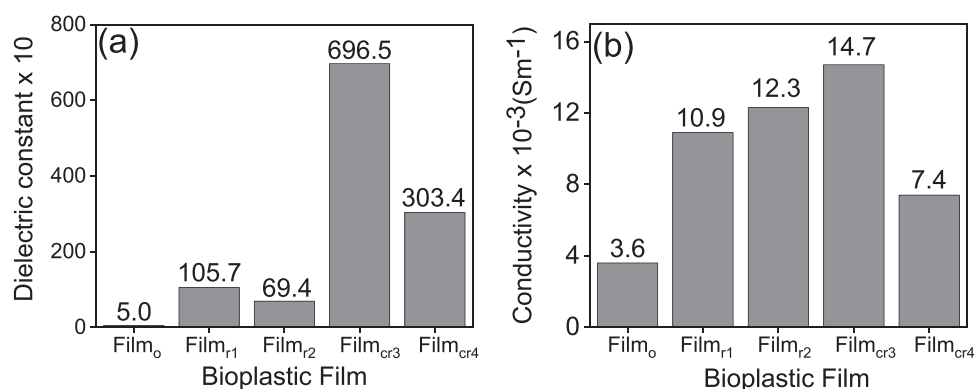


Fig. 14. (a) Dielectric constant and (b) Electrical conductivity of the bioplastic films.

Appendix A. Supporting information

Supplementary data associated with this article can be found in the online version at doi:10.1016/j.scenv.2024.100093.

References

- [1] A. Amri, H. Rahmana, S.P. Utami, R.S. Iriyanti, Z.T. Jiang, M.M. Rahman, Conductive composites of tapioca-based bioplastic and electrochemical-mechanical liquid exfoliation (emle) graphene, *I. O. P. Conf. Ser. Mater. Sci. Eng.* 345 (2018) 1–11.
- [2] S. Mahmud, K.M.F. Hasan, M.A. Jahid, K. Mohiuddin, R. Zhang, J. Zhu, Comprehensive review on plant fiber-reinforced polymeric biocomposites, *J. Mater. Sci.* 56 (2021) 7231–7264.
- [3] K.E. Rivadeneira-Velasco, C.A. Utreras-Silva, A. Díaz-Barrios, A.E. Sommer-Márquez, J.P. Tafur, R.M. Michell, Green nanocomposites based on thermoplastic starch: a review, *Polym. (Basel)* (2021) 1–36.
- [4] J.G. Rosenboom, R. Langer, G. Traverso, Bioplastics for a circular economy, *Nat. Rev. Mater.* (2022) 117–137.
- [5] I.B. Basumatary, A. Mukherjee, V. Katiyar, S. Kumar, Biopolymer-based nanocomposite films and coatings: recent advances in shelf-life improvement of fruits and vegetables, *Crit. Rev. Food Sci. Nutr.* (2022) 1912–1935.
- [6] A. Barra, J.D.C. Santos, M.R.F. Silva, C. Nunes, E. Ruiz-Hitzky, I. Gonçalves, S. Yıldırım, P. Ferreira, P.A.A.P. Marques, Graphene derivatives in biopolymer-based composites for food packaging applications, *Nanomaterials* 10 (2020) (2020) 1–32.
- [7] H. Tian, H. Zhou, H. Fu, X. Li, W. Gong, Enhanced electrical and dielectric properties of plasticized soy protein bioplastics through incorporation of nanosized carbon black, *Polym. Compos.* 41 (2020) 5246–5256.
- [8] M. Jiménez-Rosado, E. Bouroudian, V. Perez-Puyana, A. Guerrero, A. Romero, Evaluation of different strengthening methods in the mechanical and functional properties of soy protein-based bioplastics, *J. Clean. Prod.* 262 (2020) 1–7.
- [9] Z.N. Diyana, R. Jumaidin, M.Z. Selamat, I. Ghazali, N. Julmohammad, N. Huda, R. A. Ilyas, Physical properties of thermoplastic starch derived from natural resources and its blends: a review, *Polymers* 13 (2021) 5–20.
- [10] A.A. Arrieta, P.F. Ganán, S.E. Márquez, R. Zuluaga, Electrically conductive bioplastics from cassava starch, *J. Braz. Chem. Soc.* 22 (2011) 1170–1176.
- [11] A. Kausar, Polyaniline/graphene nanoplatelet nanocomposite towards high-end features and applications, *Mat. Res. Inno.* 26 (2022) 249–261.
- [12] A.R. Marlinda, M.N. Anam, N. Yusoff, S. Sagadevan, Y.A. Wahab, M.R. Johan, Recent progress in nitrates and nitrites sensor with graphene-based nanocomposites as electrocatalysts, *Trends Environ. Anal. Chem.* 34 (2022) 1–12.
- [13] I. Roy, G. Sarkar, S. Mondal, D. Rana, A. Bhattacharyya, N.R. Saha, A. Adhikari, D. Khastgir, S. Chattopadhyay, D. Chattopadhyay, Synthesis and characterization of graphene from waste dry cell battery for electronic applications, *RSC Adv.* 6 (2016) 10557–10564.
- [14] H. Bai, B. Zhang, X. Cheng, J. Liu, X. Wang, W. Qin, M. Zhang, Synthesis of zwitterionic polymer modified graphene oxide for hydrophilic enrichment of N-glycopeptides from urine of healthy subjects and patients with lung adenocarcinoma, *Talanta* 237 (2022) 1–8.
- [15] C. Fu, Q. Ma, H. Liu, W. Tang, Effects of graphene oxide on the conductivity and capacitance of polypyrrole, *Int. J. Electrochem. Sci.* 13 (2018) 4267–4275.
- [16] P. Das, A.B. Deoghare, S.R. Maity, Fabrication and characterization of polyaniline (PANI) modified with reduced graphene oxide (R.G.O.) nanosheets, *Mater. Today Proc.* 72 (2023) 2306–2314.
- [17] S. Bandi, S. Ravuri, D.R. Peshwe, A.K. Srivastav, Graphene from discharged dry cell battery electrodes, *J. Hazard. Mater.* 366 (2019) (2019) 358–369.
- [18] P. Kuchhal, U.C. Sharma, Solid Waste Management, in: Gurjar BR, Sharma UC Singh N (Eds.), *Battery Waste Management*, Studium Press L.L.C, Texas, 2017, pp. 141–155.
- [19] Y. Pan, V. Lo, L. Cao, A. Roy, B. Chivers, N. Noorbekesht, Y. Yao, J. Wang, L. Wei, Chen, Graphitic carbon from catalytic methane decomposition as efficient conductive additives for zinc-carbon batteries, *Carbon* 192 (2022) 84–92.
- [20] R.A. Mahdi, Y. Bahrami, E. Kakaei, Identification and antibacterial evaluation of endophytic actinobacteria from *Luffa cylindrica*, *Sci. Rep.* 12 (2022) 1–13.
- [21] C.A. Adeyanju, S. Ogundeyi, J.O. Igahlo, A.G. Adeniyi, S.A. Abdulkareem, A review on Luffa fibres and their polymer composites, *J. Mater. Sci.* 56 (2021) 2797–2813.
- [22] A. Adewuyi, F.V. Pereira, Isolation and surface modification of Cellulose from underutilized *Luffa cylindrica* sponge: a potential feed stock for local polymer industry in Africa, *J. Assoc. Arab Univ. Basic Appl. Sci.* 24 (2017) 39–45.
- [23] Y. Seki, K. Sever, S. Erden, M. Sarikanat, G. Nesan, C. Ozes, Characterization of *Luffa cylindrica* fibers and the effect of water aging on the mechanical properties of its composite with polyester, *J. Appl. Polym. Sci.* 123 (2012) 2330–2337.
- [24] N. Mohanta, S.K. Acharya, Effect of alkali treatment on the flexural properties of a *Luffa cylindrica*-reinforced epoxy composite, *Sci. Eng. Compos* 25 (2018) 85–93.
- [25] Agustin, B. Melissa, P. E. Richel, J. L. De Leon, Beunaobra, M. S. Marie, M. F. Alonzo, Patriana, F Hirose, B. Ahmad "Starch based bioplastics reinforced with cellulose nanocrystals from agricultural residues. In Int. Conf. on Adv in Eng and Tech. (2014) 593–597.
- [26] C.C. Coelho, M.A. Cerqueira, R.N. Pereira, L.M. Pastrana, O. Freitas-Silva, A. Vicente, L.M.C. Cabral, J.A. Teixeira, Effect of moderate electric fields in the properties of starch and chitosan films reinforced with microcrystalline Cellulose, *Carbohydr. Polym.* 174 (2017) 1181–1191.
- [27] X. Li, L. Meng, Y. Zhang, Z. Qin, L. Meng, C. Li, M. Liu, Research and application of polypropylene carbonate composite materials: a review, *Polym. (Basel)* 14 (2022) 1–23.
- [28] N. Soyeakbaew, N. Tawichai, M. Fah, O. Suwantong, Nanocellulose-reinforced "green" composite materials Biopolymers for wound dressing, *Walailak J. Sci. Tech.* 14 (2017) 353–368.
- [29] J. Tropp, J. Rivnay, Design of biodegradable and biocompatible conjugated polymers for bioelectronics, *J. Mater. Che. C.* 9 (2021) 13543–13556.
- [30] S. Ramanavicius, A. Ramanavicius, Conducting polymers in the design of biosensors and biofuel cells, *Polymers* 13 (2020) 49–55.
- [31] N. Dubey, C.S. Kushwaha, S.K. Shukla, A review on electrically conducting polymer nanocomposites for biomedical and other applications, *Int. J. Polym. Mater. Polym. Biomater.* (2019) 1–19.
- [32] O.O. Oluwasina, F.K. Olaleye, S.J. Olusegun, O.O. Oluwasina, N.D.S. Mohalle, Influence of oxidized starch on physicomechanical, thermal properties, and atomic force micrographs of cassava starch bioplastic film, *Int. J. Biol. Macromol.* 135 (2019) 282–293.
- [33] O.O. Oluwasina, L. Lajide, B.J. Owolabi, Performance of bonded boards using lignin-based resins, *Wood Mater. Sci. Eng.* 10 (2015) 168–177.
- [34] W.S. Hummers, R. E. Offerman RE preparation of graphitic oxide, *J. Am. Chem. Soc.* 80 (1958) 1339.
- [35] O.O. Oluwasina, T. Falola, O.J. Wahab, N.B. Idahagbon, enhancement of physical and mechanical properties of *Dioscorea dumetorum* starch films with dialdehyde starch solution, *Starch/Starke* 1700148 (2017) 1–7.
- [36] M. Jiménez-Rosado, J.E. Maigret, D. Lourdin, A. Guerrero, A. Romero, Injection molding versus extrusion in the manufacturing of soy protein-based bioplastics with zinc incorporated, *J. Appl. Polym. Sci.* 139 (2022) 1–14.
- [37] J. Yang, X. Dong, J. Wang, Y.C. Ching, J. Liu, L. Chunhui, Y. Baikeli, Z. li, Mohammed N. Al-Hada, S. Xu, Synthesis and properties of bioplastics from corn starch and citric acid-epoxidized soybean oil oligomers, *J. Mater. Res. Technol.* 20 (2022) 373–380.
- [38] G. Papa, M. Cucina, K. Echchouki, P. De Nisi, F. Adani, Anaerobic digestion of organic waste allows recovering energy and enhancing the subsequent bioplastic degradation in soil, *Resour. Conserv. Recycl.* 188 (2023) 1–9.
- [39] Z. Chen, M. Deng, Y. Chen, G. He, M. Wu, J. Wang, Preparation and performance of cellulose acetate/polyethylenimine blend microfiltration membranes and their applications, *J. Membr. Sci.* 235 (2004) 73–86.
- [40] S.S. Rumi, S. Liyanage, N. Abidi, Conversion of low-quality cotton to bioplastics, *Cellulose* 28 (2021) 2021–2038.
- [41] American Society for Testing and Materials. Standard Test Method for Tensile Properties of Thin Plastic Sheeting. Designation: D882 – 10: ASTM-D882-2010_513100089384.
- [42] A. Rani, S.W. Nam, K.A. Oh, M. Park, Electrical conductivity of chemically reduced graphene powders under compression, *Carbon Lett.* 11 (2010) 90–95.
- [43] W.P. Flauzino Neto, H.A. Silvério, N.O. Dantas, D. Pasquini, Extraction and characterization of cellulose nanocrystals from agro-industrial residue - Soy hulls, *Ind. Crops Prod.* 42 (2013) 480–488.
- [44] J. Wang, E.C. Salih, L. Siller, Green reduction of graphene oxide using alanine, *Mater. Sci. Eng. C* 72 (2017) 1–6.
- [45] A.V. Talyzin, Random interstratification in hydrated graphene oxide membranes and implications for seawater desalination, *Nat. Nanotechnol.* 17 (2022) 131–133.
- [46] K. Sakthi Velu, M. Alam, N. Ahmad, S. Esakkimuthu, G. Vignesh Kumar, S. Mohandas, J. Anandha Raj, K. Selvam, G. Kalita, T. Stalin, Photo-anode surface modification using novel graphene oxide integrated with methylammonium lead iodide in organic-inorganic perovskite solar cells, *J. Phys. Chem. Solids* 154 (2021) 1–8.
- [47] R.L. Razalli, M.M. Abdi, P.M. Tahir, A. Moradbak, Y. Sulaiman, L.Y. Heng, Polyaniiline-modified nanocellulose prepared from Semantan bamboo by chemical polymerization: Preparation and characterization, *RSC Adv.* 7 (2017) 25191–25198.
- [48] M.S. Bhutta, T. Xuebang, S. Akram, C. Yidong, X. Ren, M. Fasehullah, G. Rasool, M. T. Nazir, Development of novel hybrid ²D–³D graphene oxide diamond micro composite polyimide films to ameliorate electrical & thermal conduction, *J. Ind. Eng. Chem.* 114 (2022) 108–114.
- [49] P. Tambe, Synthesis and characterization of acid-treated reduced graphene oxide, : *Mater. Today.: Proc.* 49 (2021) 1294–1297.
- [50] Q.A. Khan, A. Shaur, T.A. Khan, Y.F. Joya, M.S. Awan, Characterization of reduced graphene oxide produced through a modified Hoffman method, *Cogent Chem.* 3 (2017) 1–9.
- [51] O. Z. Farinre, H. Alghamdi, S.M. Mhatre, M.L. Kelley, A.J. Biacchi, A. V. Davydov, C.A. Hacker, A.F. Rigosi, P. Misra, Comprehensive Data via Spectroscopy and Molecular Dynamics of Chemically Treated Graphene Nanoplatelets, *Data (Basel)* 7 (2022) 1–16.
- [52] Y. Wu, Y. Ma, Y. Wang, L. Huang, N. Li, T. Zhang, Y. Zhang, X. Wan, Y. Huang, Y. Chen, Efficient and large scale synthesis of graphene from coal and its film electrical properties studies, *J. Nanosci. Nanotech.* 13 (2013) 929–932.
- [53] F.W. Low, C.W. Lai, S.B. Abd Hamid, Easy preparation of ultrathin reduced graphene oxide sheets at a high stirring speed, *Ceram. Int.* 41 (2015) 5798–5806.
- [54] P. Jiang, L. Zhou, W. Wang, N. Li, F. Zhang, Performance and mechanisms of fly ash for graphene oxide removal from aqueous solution, *Environ. Sci. Pollut. Res.* 29 (2022) 3773–3783.
- [55] J.T. Mhlongo, T. Nuapia, M.M. Motsa, T.O. Mahlangu, A. Etale, Green chemistry approaches for extraction of cellulose nanofibers (C.N.F.s): a comparison of mineral and organic acids, *Mater. Today Proc.* 62 (2022) S57–S62.

- [56] J.C.C.C. Benini, H.J.C. Voorwald, M.O.H. Cioffi, M.C. Rezende, V. Arantes, Preparation of nanocellulose from Imperata brasiliensis grass using Taguchi method, *Carbohydr. Polym.* 192 (2018) 337–346.
- [57] E. Aliyev, V. Filiz, M.M. Khan, Y.J. Lee, C. Abetz, V. Abetz, Structural characterization of graphene oxide: surface functional groups and fractionated oxidative debris, *Nanomaterials* 9 (2019) 1–15.
- [58] S.N. Alam, N. Sharma, L. Kumar, Synthesis of graphene oxide (G.O.) by modified hummers method and its thermal reduction to obtain reduced graphene oxide (rGO), *Graphene* 6 (2017) 1–18.
- [59] G.A.S. Juárez, E.G. Barojas, E. Quiroga-González, E. Sánchez-Mora, J. D. Santamaría-Juárez, Preparation and characterization of reduced graphene oxide/titanium dioxide composites by hydrothermal method, *Eur. J. Eng. Sci. Tech.* 4 (2019) 165–173.
- [60] M.K. Marichelvam, P. Manimaran, M.R. Sanjay, S. Siengchin, M. Geetha, K. Kandakodeeswaran, P. Boonyasopon, S. Gorbatyuk, Extraction and development of starch-based bioplastics from Prosopis juliflora Plant: eco-friendly and sustainability aspects, *Curr. Res. Green. Sustain. Chem.* 5 (2022) 1–9.
- [61] Q. Wang, J. Yan, Z. Fan, Carbon materials for high volumetric performance supercapacitors: design, progress, challenges and opportunities, *Energy Environ. Sci.* 9 (2016) 729–762.
- [62] T. Maulida, M.B. Kartika, M.H.S. Harahap, Ginting, Utilization of mango seed starch in manufacture of bioplastic reinforced with microparticle clay using glycerol as plasticizer, *I. O. P. Conf. Ser.: Mater. Sci. Eng.* 309 (2018) 1–8.
- [63] M. Ghasemlou, N. Aliheidari, R. Fahmi, S. Shojaee-Aliabadi, B. Keshavarz, M. J. Cran, R. Khaksar, Physical, mechanical and barrier properties of corn starch films incorporated with plant essential oils, *Carbohydr. Polym.* 98 (2013) 1117–1126.
- [64] P.C. Belibi, T.J. Daou, J.M.B. Ndjaka, B. Nsom, L. Michelin, B. Durand, A comparative study of some properties of cassava and tree cassava starch films, *Phys. Procedia* 55 (2014) 220–226.
- [65] D. Shan, E. Gerhard, C. Zhang, J.W. Tierney, D. Xie, Z. Liu, J. Yang, Polymeric biomaterials for biophotonic applications, *Bioact. Mater.* 3 (2018) 434–445.
- [66] F.G. Nugroho, N.M. Nizardo, E. Saepudin, Synthesis of citric acid crosslinked P.V. A./tapioca starch bioplastic reinforced with grafted cellulose, *A. I. P. Conf. Proc. 2242* (2020) 1–8.
- [67] J. Ma, X. Wang, T. Wu, Y. Liu, Y. Guo, R. Li, X. Sun, F. Wu, C. Li, J. Gao, Y. Liu, Reduction of graphene oxide with l-lysine to prepare reduced graphene oxide stabilized with polysaccharide polyelectrolyte, *J. Mater. Chem. A Mater.* 1 (2013) 2192–2201.
- [68] A.A.S. Curvelo, A.J.F. De Carvalho, J.A.M. Agnelli, Thermoplastic starch-cellulosic fibers composites: Preliminary results, *Carbohydr. Polym.* 45 (2001) 183–188.
- [69] W. Ban, J. Song, D.S. Argyropoulos, L.A. Lucia, Improving the physical and chemical functionality of starch-derived films with biopolymers, *J. Appl. Polym. Sci.* 100 (2006) 2542–2548.
- [70] M. Gaspar, Z. Benko, G. Dogossy, K. Reczey, T. Czigány, M. Gáspár, Z. Benko, G. Dogossy, K. Réczey, T. Czigány, Reducing water absorption in compostable starch-based plastics, *Polym. Degrad. Stab.* 90 (2005) 563–569.
- [71] T. Kuila, A.K. Mishra, P. Khanra, N.H. Kim, J.H. Lee, Recent advances in the efficient reduction of graphene oxide and its application as energy storage electrode materials, *Nanoscale* 5 (2013) 52–71.
- [72] X. Fang, C. Wang, H. Li, X. Wang, S. Zhang, X. Luo, H. Jia, Influence of mesoscopic pore characteristics on the splitting-tensile strength of cellular concrete through deep-learning based image segmentation, *Constr. Build. Mater.* 315 (2022) 1–12.
- [73] R.F. Santana, R.C.F. Bonomo, O.R.R. Gandolfi, L.H. Rodrigues, L.S. Santos, A.C. dos Santos Pires, C.P. de Oliveira, R. da Costa Ilhéu Fontan, C.M. Veloso, Characterization of starch-based bioplastics from jackfruit seed plasticized with glycerol, *J. Food Sci. Technol.* 55 (2018) 278–286.
- [74] G.S. Juárez, E. Gómez, E.Q. González, E. Sánchez, S. Juárez, *Prep. Charact. Reduc. Graph. Oxide / Titan. Dioxide Compos. Hydrothermal Method* 4 (2019) 165–173.
- [75] L.O. Ekebafea, G.O. Adebayo, M.N. Chukwua, K.O. Eguare, Performance evaluation of graphite oxide in natural rubber compounds, *Niger. J. Chem. Res.* 24 (2019) 20–33.
- [76] P.S.D.O. Patrício, F.V. Pereira, M.C. dos Santos, P.P. de Souza, J.P.B. Roa, R. L. Oreifice, Increasing the elongation at break of polyhydroxybutyrate biopolymer: effect of cellulose nanowhiskers on mechanical and thermal properties, *J. Appl. Polym. Sci.* 127 (2013) 3613–3621.
- [77] R. Arjmandi, N. Suib, A. Hassan, I.I. Muhamad, N. Pa'a, Z. Zakaria, Tensile and morphological properties of bacterial cellulose nanowhiskers reinforced polylactic acid nanocomposites, *Chem. Eng. Trans.* 56 (2017) 1327–1332.
- [78] N. Gómez-Gast, M.D.R.L. Cuellar, B. Vergara-Porras, H. Vieyra, Biopackaging potential alternatives: bioplastic composites of polyhydroxyalkanoates and vegetal fibers, *Polym. (Basel)* 14 (2022) 1–24.
- [79] M. Devi, A. Kumar, Thermal, electrical, and dielectric properties of reduced graphene oxide-polyaniline nanotubes hybrid nanocomposites synthesized by in situ reduction and varying graphene oxide concentration, *J. Appl. Polym. Sci.* 135 (2018) 1–11.
- [80] A. Salea, R. Saputra, C. Putson, Enhanced interfacial dielectric polarization in PVDF-HFP copolymer with treating PPy by using silane coupling agent, in: *I.O.P. Conference Series: Materials Science and Engineering.*, 773, Institute of Physics Publishing, 2020, pp. 1–5.
- [81] G.F.V. Ayissi Eyebe, B. Bideau, E. Loranger, F. Domingue, TEMPO-oxidized cellulose nanofibre (T.O.C.N.)films and composites with P.V.O.H. as sensitive dielectrics for microwave humidity sensing, *Sens. Actuators B Chem.* 291 (2019) 385–393.
- [82] Z. Alves, N.M. Ferreira, P. Ferreira, C. Nunes, Design of heat sealable starch-chitosan bioplastics reinforced with reduced graphene oxide for active food packaging, *Carbohydr. Polym.* 291 (2022) 1–11.